A Submillimeter High Angular Resolution Bolometer Array Camera for the Caltech Submillimeter Observatory

N. Wang, T.R. Hunter, D.J. Benford, E. Serabyn, D.C. Lis, T.G. Phillips

California Institute of Technology, M/S 320-47, Pasadena, CA 91125

S.H. Moseley, K. Boyce, A. Szymkowiak, C. Allen, B. Mott, J. Gygax

NASA Goddard Space Flight Center, Greenbelt, MD 20771

Abstract

We have constructed a bolometer array camera optimized for the 350 μm and 450 μm atmospheric windows for the Caltech Submillimeter Observatory (CSO). The detectors are micromachined monolithic silicon thermal bolometers cooled to 300 mK by a ^{3}He refrigerator. They form a close-packed linear array of 24 bolometers which provide Nyquist sampling of the diffraction pattern from the CSO in a strip 10"x2' on the sky. The bolometers achieve a Noise Equivalent Power of $5 \cdot 10^{-15}\ W/\sqrt{Hz}$, which is approximately background limited in good Mauna Kea weather. Liquid Helium cooled optics provide the aperture and field stops and reimage the sky onto the bolometer array, eliminating the need for Winston cones. The total optical efficiency of the camera is ≈10%. Several successful runs at the CSO have proven the ability of this instrument to allow significantly better and faster mapping of astronomical sources than was previously possible.

1. Introduction

In order to better understand the process of star formation and the evolution of galaxies, it is sometimes necessary to make continuum observations of dust emission at submillimeter wavelengths over a sizable area. This goal is well fit by a broadband detector with imaging capabilities operating at submillimeter wavelengths, which has the obvious advantage of increasing the efficiency of the telescope as compared to the single element detector presently available at the CSO; it can also allow better reduction of sky noise.

We have constructed a continuum camera for the Caltech Submillimeter Observatory (CSO), operating in the 350 μm and 450 μm atmospheric window[1]. It employs a monolithic linear Silicon bolometer array fabricated by the microelectronics laboratory at the Goddard Space Flight Center (GSFC). The array has 24 bolometer pixels which are 1 mm wide and separated by about 15 μm. No Winston cones[2] are used in the camera; instead, we use off-axis elliptical mirrors to reimage the sky onto the bolometer array, and aperture and field stops to define the beam.

We have designed the optics such that each pixel subtends 5 arcseconds by 10 arcseconds on the sky. The CSO has a 10.4 m diameter primary mirror, yielding a diffraction beamwidth of 10 arcseconds at 400 μm, so that the pixels Nyquist sample the diffraction pattern along the array.

As in a conventional bolometer instrument, cooled FETs are used in the first stage of amplification, followed by room temperature amplifiers. Signals from the output of these amplifiers are digitized at 1 kHz. Each bolometer has its own analog to digital converter (A/D), so that all the signals are digitized simultaneously. A special digital signal processing (DSP) board, designed by A. Szymkowiak, K. Boyce, R.G. Baker, S.H. Moseley, W. Folz, and R.F. Lowenstein, performs the digital lock-in measurement, as it is very costly to use analog lock-in amplifiers for 24 channels. To isolate digital noise from the computer, fiber optic cables are used to transmit the digital signal from the A/Ds to the DSP board. The DSP board is situated inside a backend computer assigned to the camera. Direct lines are used for communication between the backend computer, the antenna control computer, and the telescope control computer to monitor the timing of the idle and acquire states of the telescope, while data is sent from the backend computer to the telescope control computer via Ethernet.

We have fully tested the camera in the laboratory, and have successfully operated the camera on the telescope. In the 450 μm window, the optical responsivity is about $9 \cdot 10^6$ V/W, the total quantum efficiency is 9%, and the optical noise equivalent power (NEP) is $6 \cdot 10^{-15}$ $W/\sqrt{Hz}$. In the 350 μm window, the optical responsivity is about $1 \cdot 10^7$ V/W, the total quantum efficiency is 10%, and the optical NEP is $5 \cdot 10^{-15}$ $W/\sqrt{Hz}$. The noise equivalent flux density (NEFD) is 4 $Jy/\sqrt{Hz}$ in good weather. The camera is diffraction limited optically.

2. Monolithic Bolometer Array

A. Structure

The bolometer array used in this camera (Figure 1) is a monolithic silicon array fabricated in the microelectronics laboratory at GSFC[3]. There are 24 pixels in the array, and the gap between adjacent pixels is about 15 μm. Each pixel is suspended by four long thin silicon legs, formed by wet chemical etching; these thin legs provide a weak thermal link between the pixels and the heat sink, which is important in order to have a sensitive bolometer. The pixels are 1 mm x 2 mm x 12 μm, and the thin legs are 12 μm x 14 μm x 2 mm. The entire array is micromachined from a single silicon wafer.

Each pixel is a composite bolometer (Figure 2), consisting of an absorber and a thermistor. The thermistor is deposited onto each pixel by phosphorus implantation with boron compensation; the doping has an appropriate density so that the thermistor's resistance at 300 mK is on the order of 10 MΩ. Electrical leads are implanted along two of the suspending silicon legs leading to the contact pads used for wire bonding.

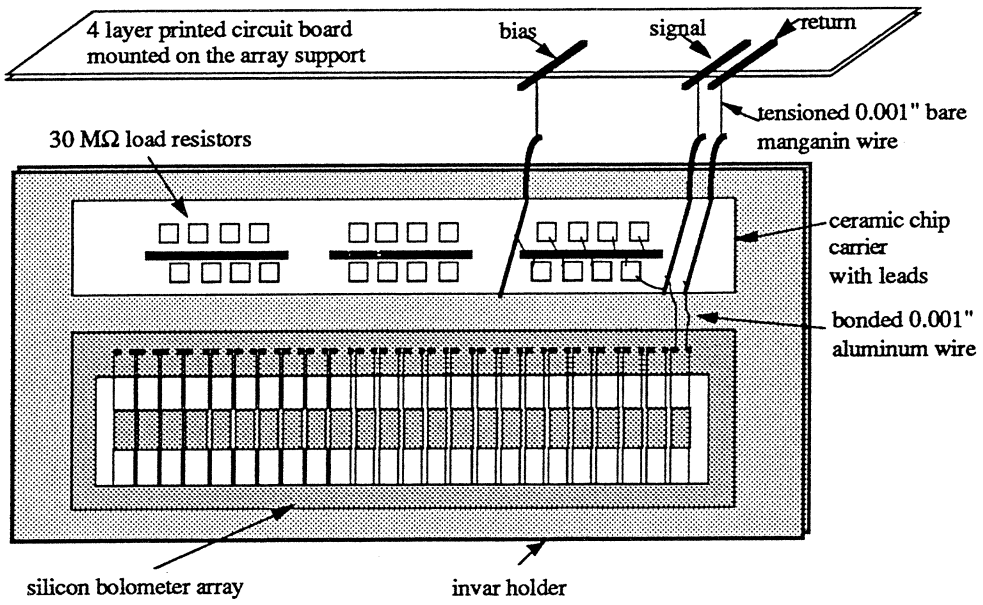

Figure 1. Layout of the 24 element bolometer array.

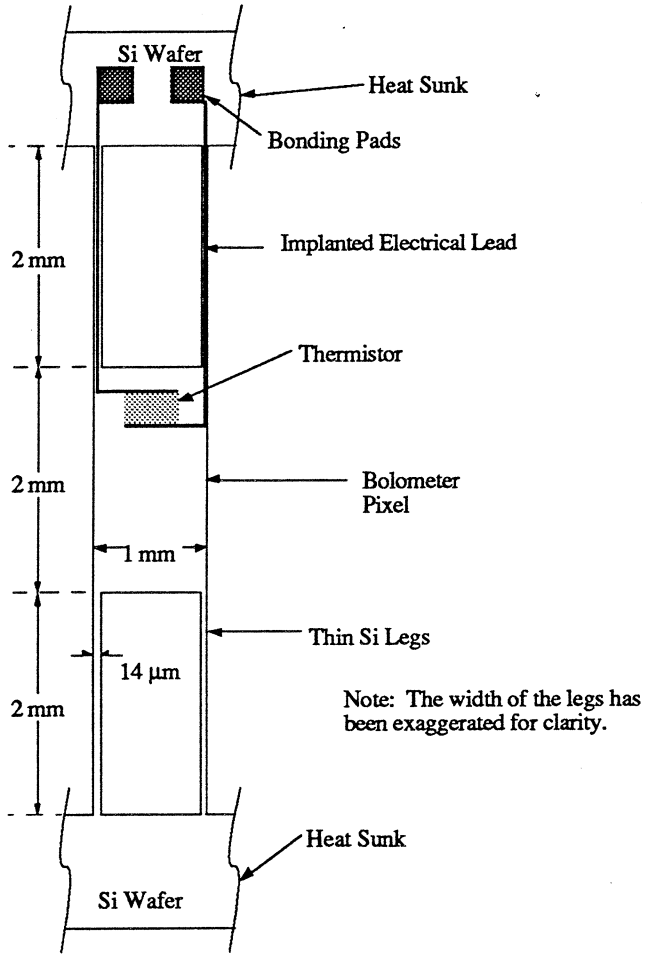

Figure 2. Schematic drawing of a single bolometer pixel.

Because silicon does not absorb submillimeter radiation, a bismuth film about 1100 Å thick is evaporated on the back of all the bolometer pixels, followed by 200 Å of SiO to protect the bismuth. The bismuth thickness was chosen to optimize the pixel's absorptivity, which is at best 50%, by attempting to have an electrical impedance at the operating temperature which matches that of the free space[4]. However, the impedance of the bismuth film on our array, measured at 4 K, gives an estimated absorptivity of around 35%, leaving some room for improvement.

B. Electrical Circuit

As in a conventional bolometer circuit[5], the thermistor in each bolometer pixel is voltage biased in series with a 30 MΩ metal film load resistor (Figure 3), which is kept at the ^{3}He bath temperature on the same invar mount as the array. Signals from the thermistors are sent to cryogenically cooled FETs, which are connected as source followers. Signals from the FETs are then sent to the input of room temperature amplifiers.

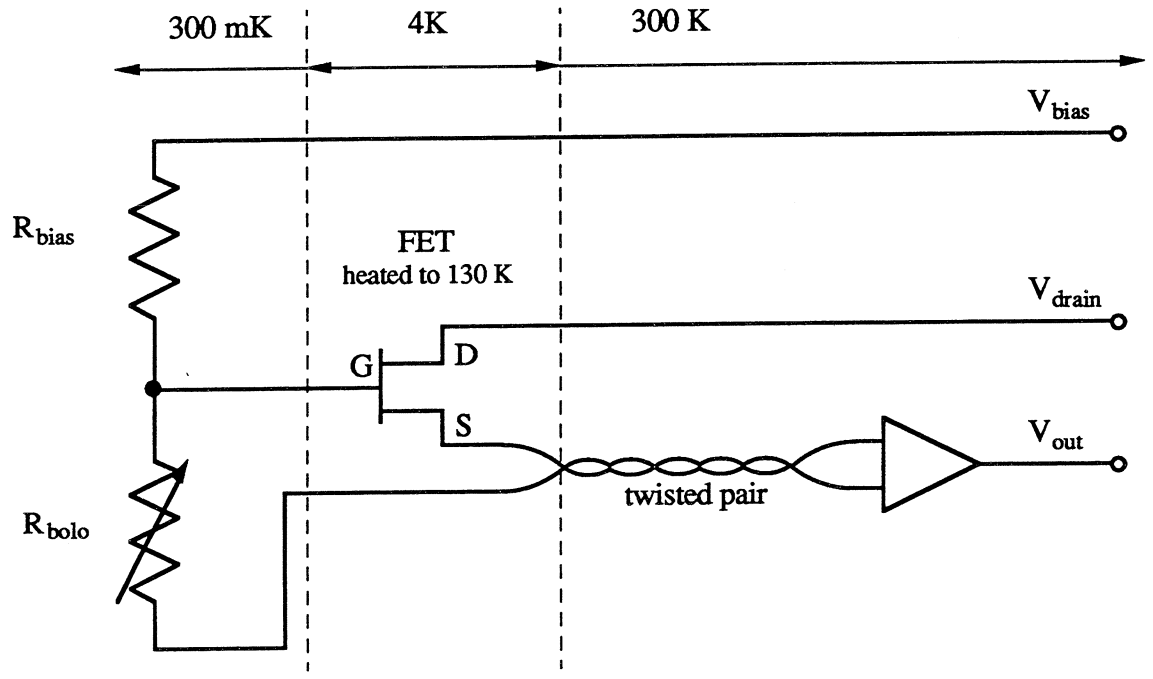

Figure 3. Circuit diagram of a bolometer pixel.

C. Array Suspension and Thermal Isolation

The mechanical design of the instrument is important, as we must thermally isolate parts at different temperatures from one another, while keeping wiring lengths short and avoiding coupling mechanical vibrations to the signal wires and the thermistors.

The bolometer array is attached to an Invar holder, using a single spot of glue at one point in order to avoid thermal stress. Invar is used because, like Silicon, it has very little thermal contraction from room temperature to cryogenic temperatures. All the load resistors are glued to a ceramic flatpack, which is glued to the Invar holder. The holder is cooled to the ^{3}He temperature by a copper cold finger. Electrical connections between the thermistors

and the load resistors are made by ultrasonically bonding 0.001 inch aluminum wires between the contact pads on the array and the leads on the ceramic flatpack. The Invar holder is suspended with spring-loaded Kevlar threads from an aluminum array support which is mounted to the frame of the radiation baffle box (Figure 5) and is maintained at the helium bath temperature. Kevlar is a very poor thermal conductor[6], and therefore provides thermal isolation between the array support and the Invar. The Kevlar threads are spring loaded to make the frequency of microphonic noise higher than that of the signals, i.e., above 10 Hz. The electrical connections between the 300 mK and 1.5 K stages are made by soldering 0.001 inch diameter bare manganin wires between them, maintaining the wires under tension in order to minimize any possible microphonic noise in the frequency range of interest.

D. Electrical Properties: R(T)

In order to understand the performance of a bolometer, it is crucial to know the temperature dependence of the thermistor's resistance. Based on the doping level of our thermistors, we expect that the resistance be due to variable range hopping, giving rise to a zero bias resistance of the form[7]

$$R(T) = R_0 \exp\sqrt{\frac{T_0}{T}} \qquad (1)$$

where $R(T)$ is the thermistor's resistance at temperature T, and R_O and T_O are constants specific to the thermistor.

The zero bias resistance is measured by taking the current-voltage (I-V) characteristic curve of a bolometer. An I-V curve is obtained by applying a bias voltage, supplied by a battery, to the load resistor in series with the bolometer, and simultaneously recording the bias voltage and the voltage across the bolometer pixel, using the data acquisition system described later in this paper. In Figure 3 we show some typical I-V curves of eight bolometer pixels taken simultaneously at a ^{3}He bath temperature of 298 mK. One can see from the data that the I-V curves of all eight pixels are very similar, as are their zero bias resistances. The shifts in the I-Vs between different pixels indicate different thermoelectric voltages for each pixel. From I-Vs taken at different ^{3}He temperatures, one can obtain the zero bias resistance as a function of temperature.

In Figure 4, we show the measured zero bias resistance at different temperatures for three pixels. We show also the corresponding fits to Equation (1), which describes the temperature dependence of the zero bias resistance rather well. The fact that three different pixels have similar temperature dependence indicates that the pixels have similar electrical properties, an important feature required for an array used in a camera.

E. Thermal Properties: G(T)

In addition to the electrical behavior of a bolometer, it is important to understand its thermal conductance. In this section, we will describe the measured thermal conductance of the bolometer, $G(T)$, and compare it with the expected value.

One can obtain the thermal conductance of a bolometer from the I-V characteristic curve if one assumes that the bolometer resistance at any bias point, $R = V/I$, gives the temperature of the bolometer according to the formula

for the zero bias resistance (Equation 1). At any bias point *(I,V)*, one can then calculate the temperature of the bolometer from

$$T = T_0\left(\ln\left[R/R_0\right]\right)^{-2} \qquad (2)$$

where R_O and T_O are known from measuring the temperature dependence of the zero bias resistance. An I-V curve can then be replotted in terms of bias power $P = IV$ as a function of the bolometer temperature, which then gives the thermal conductance of the bolometer as a function of temperature, $G(T) = \frac{dP}{dT}$.

In Figure 5, we show bias power P as a function of $T^4 - T_{sink}^4$, where T_{sink} is the temperature of the heat sink, the ^{3}He bath temperature. The data show that P is proportional to $T^4 - T_{sink}^4$, giving rise to a thermal conductance *G(T)*:

$$G(T) = \frac{dP}{dT} = 3.2 \cdot 10^{-8} T^3 \ \text{(W/K)}. \qquad (3)$$

The T^3 temperature dependence is what we expect, since the thermal conductance of the bolometer pixel is provided mostly by the four thin suspending silicon legs. Silicon is an insulator at these temperatures and thus the thermal conduction is carried by phonons, whose thermal conductance has a T^3 temperature dependence. Even though Figure 8 shows the data from only one pixel, other pixels have very similar *G(T)*. The uniformity of *G(T)* together with the uniformity of *R(T)* for all the pixels implies that the pixels will have very uniform sensitivity.

3. Electronics

In order to build a sensitive bolometer instrument, one needs to properly design the system so that one can minimize microphonic noise and electrical crosstalk between different channels. In addition, RF noise must be blocked to avoid heating the bolometers, thereby reducing their sensitivity. Finally, one has to ensure that electronic noise from the FETs and the amplifiers is low enough that the instrument's sensitivity is background limited.

A. Microphonics

The primary source of microphonic noise comes from the pump on the ^{4}He bath. Since the signal frequency is at low frequencies, as we normally chop at around 4 Hz, we need to be certain that low frequency vibrations are not coupled to the bolometers from the pump. This is realized by a careful design of the suspension and wiring of the bolometer array: the suspension is as made stiff as possible by tensioning the Kevlar support fibers, and the wires to the array are all soldered under tension. As a result, we saw no microphonic noise below 20 Hz, both in the laboratory and at the observatory.

B. RF Noise

We have done two things to try to reduce the coupling of RF noise from the environment to the bolometer array. On all the signal lines, we installed RF filters with a cutoff frequency of about 1 MHz on the electrical feedthroughs on the cryostat. In order to eliminate digital noise from the computer used to process the data, fiber

optic cables are used to transmit all signals to the computer. The fact that the measured zero bias resistance as a function of temperature gives the expected relation with no flattening at the low temperatures is a good indication that there is no significant amount of heating from RF noise. Any noticeable RF noise absorbed by the bolometer will decrease its zero bias resistance, especially at the lowest temperatures, and will make the data deviate from Equation (1).

C. Electrical Cross Talk

In order to minimize electrical crosstalk between different channels, each pixel has its own circuit ground line which is kept close to the signal line from the pixel to the input of the room temperature amplifier. Twisted pairs made of 0.005 inch diameter manganin wires are used inside the cryostat to connect from the FETs to the electrical feedthroughs on the cryostat. The grounds of all the pixels are connected together in the room temperature amplifier. At the output of the amplifier, the signals with their separate grounds are connected to the differential inputs of the A/D converters, using a cable made of twisted pairs, which has a shield for each pair. We found very little electrical crosstalk between pixels with this design.

D. Electrical Grounding

In order to avoid 60 Hz pickup, we have designed the circuit ground with great care. The room temperature amplifiers are powered by batteries. The grounds of all the channels are kept independent and floating from the cryostat. The cryostat is electrically isolated from the telescope. The circuit ground for every pixel is defined at only one point, which we chose to be the ground of the power supply for the room temperature amplifier. With this setup, we saw little 60 Hz pickup when the camera was operated at the telescope.

E. FETs

The first stage of amplification for each bolometer is a FET used as a source follower to transform the high bolometer impedance into a low source impedance. The FETs are the NJ14AL16 FETs from InterFET[6], selected at room temperature to have low noise. Because these are silicon FETs, which do not work at 4 K, they are heated to about 130 K in order to obtain the lowest noise. Eight FETs, all in their die form, are glued to a specially designed flatpack along with a heater and a diode thermometer. The flatpack is suspended from its aluminum housing with Kevlar threads kept under tension by compressed springs, which allows us to establish a temperature gradient between the flatpack at about 130 K and the housing at 1.5 K. Bare manganin wires of 0.001 inch diameter are soldered under tension between the flatpack and the connectors on the FET housing. Such small wires keeps the heat load from the FETS from noticeably affecting the bolometer impedance.

F. System Electronic Performance

The noise power spectrum of a typical bolometer is shown in Figure 4. The spectrum was recorded when the gate of the FET was connected to a bolometer pixel staring at a 4 K blankoff, biased at zero voltage and cooled to 300 mK; the source of the FET was connected to a room temperature amplifier and the FET was heated to 130 K.

The expected Johnson noise from the 30 MΩ load resistor and the zero bias resistance of the bolometer, which is around 10MΩ, is about 16 $nV/\sqrt{Hz}$. The measured noise of the room temperature amplifier at 4 Hz is 10 $nV/\sqrt{Hz}$. Figure 4 suggests that the noise of the FET itself is about 10 $nV/\sqrt{Hz}$ at 4 Hz. Note that there is no significant microphonic noise present in the noise spectrum, even though the ^{4}He bath was pumped by a mechanical pump when it was recorded.

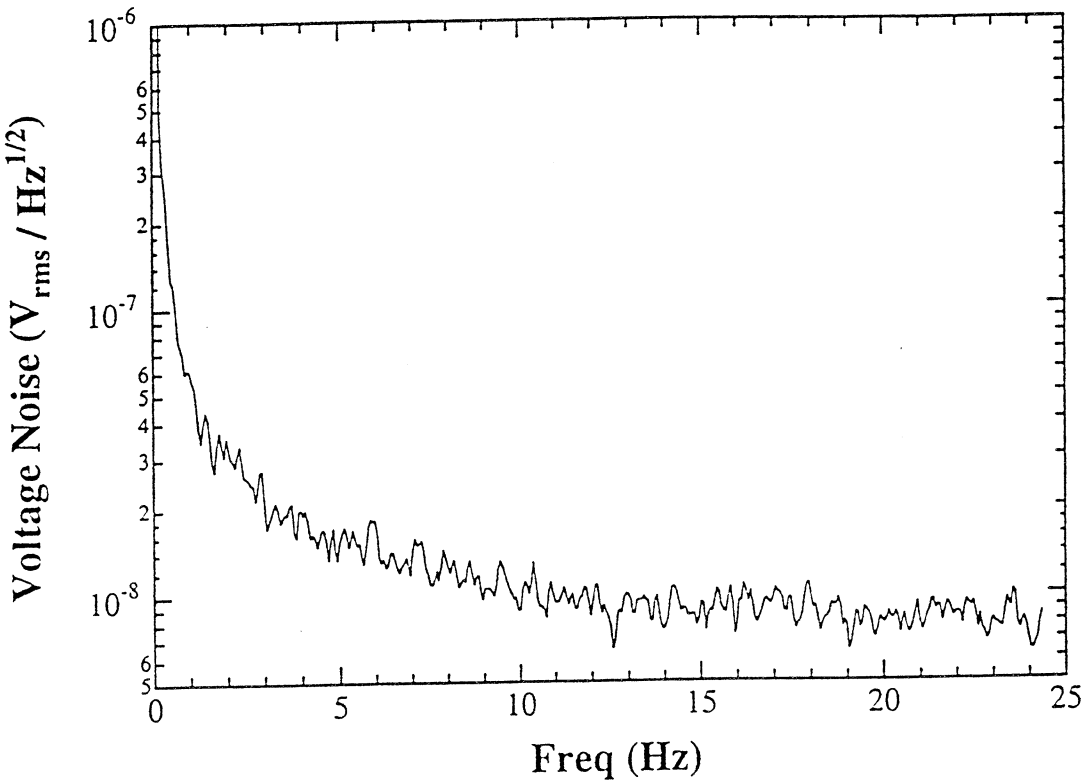

Figure 4. Noise power spectrum of the electrical system recorded in the laboratory using a spectrum analyzer.

4. Data Acquisition System

Unlike a single pixel bolometer instrument, where one can use an analog lock-in amplifier and a commercial A/D, it is rather costly to duplicate the setup for a 24 pixel array. Therefore, we built our own A/Ds for the array, using a design by R. Baker et. al. at GSFC. Lock-in detection is performed using a specially designed digital signal processing (DSP) board residing inside a Macintosh computer. Data acquisition software is written in LabView on the Macintosh, which is linked to the telescope control computer via Ethernet.

In Figure 5 we show a flow chart of the data acquisition hardware. The differential signals from the output of the room temperature amplifiers are fed to the differential inputs of the 16 bit A/Ds, which has an input range of -3V to 3V and sampling frequency of 1 kHz, but can be increased up to 40 kHz. Each channel has its own ADC chip, thus signals from all the pixels are digitized simultaneously. The output of the A/Ds are sent to the input of the DSP board using fiber optic cables, which are designed to electrically isolate the Macintosh from the instrument.

In order to synchronize the lock-in detection with the chopping secondary, a TTL signal generated by the DSP board is used to synchronize the A/D sampling and to produce the signal that drives the chopping secondary mirror. The chopping frequency can be set to 1 kHz/*n*, where 1 kHz is the A/D sampling frequency and *n* is an integer greater than 1. The A/D, therefore, samples the signal starting at the same place for every chop cycle.

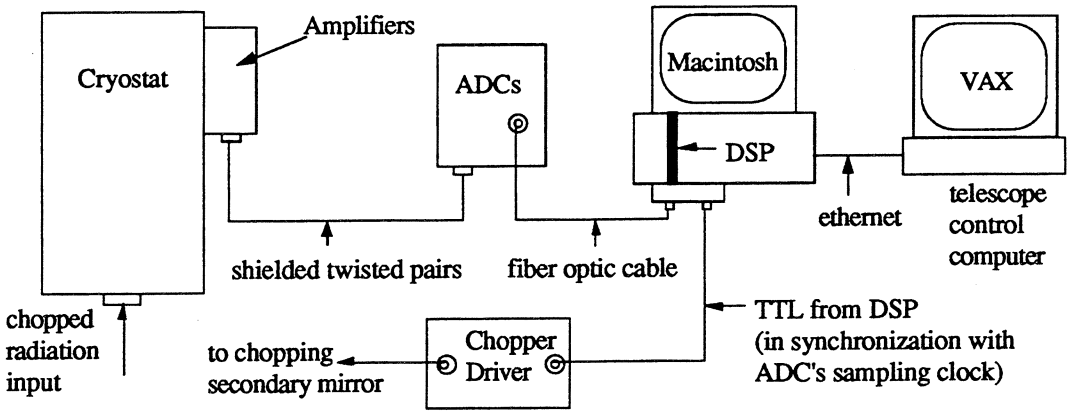

Figure 5. A diagram of the data acquisition system.

5. Cryogenics and Optics Description

A. Cryogenics

Figure 6 shows a schematic of the camera components. The cryostat, with a liquid nitrogen and liquid helium bath, is a single shot ^{3}He refrigerator with a base temperature of 295 mK. A mechanically driven heat switch is employed to control the thermal link between the ^{3}He pot and the ^{4}He bath, and a second one is used between the charcoal pump and the ^{4}He bath. Under normal operation, the ^{4}He bath is pumped with a mechanical pump, and operates at about 1.5 K. The hold time is around 18 hours on the telescope, which limits the continuous operating time of the instrument.

B. Optics Overview

One of the unique features of this instrument is the lack of beam-defining cones, as most recent bolometer systems at $\lambda > 200$ μm have relied on Winston cones. This allows us to use closely packed bolometer pixels to form an array in such a way that we achieve Nyquist sampling of the diffraction pattern at the wavelengths of interest. We use mirrors to focus the light onto the detector pixels, and an aperture stop and a field stop to define the primary illumination and the field of view, respectively.

C. Optical Components

A sheet of 1 mm thick high density polyethylene is used as the vacuum window. We chose polyethylene in order to obtain small deflection under vacuum and good transmission, ~95%, in the 350 μm and 450 μm

atmospheric windows. Undesired radiation from visible wavelengths down to about 170 μm is absorbed by a series of three infrared blocking filters, which are purchased from Infrared Labs[9], and each have about 80% transmission in the passband. On the nitrogen shield is a z-cut quartz wafer anti-reflection coated with black polyethylene on both sides. The helium shield has a z-cut quartz wafer with black polyethylene on one side and a diamond scatter layer on the other, followed by a CsI filter with clear polyethylene antireflection coating on both sides.

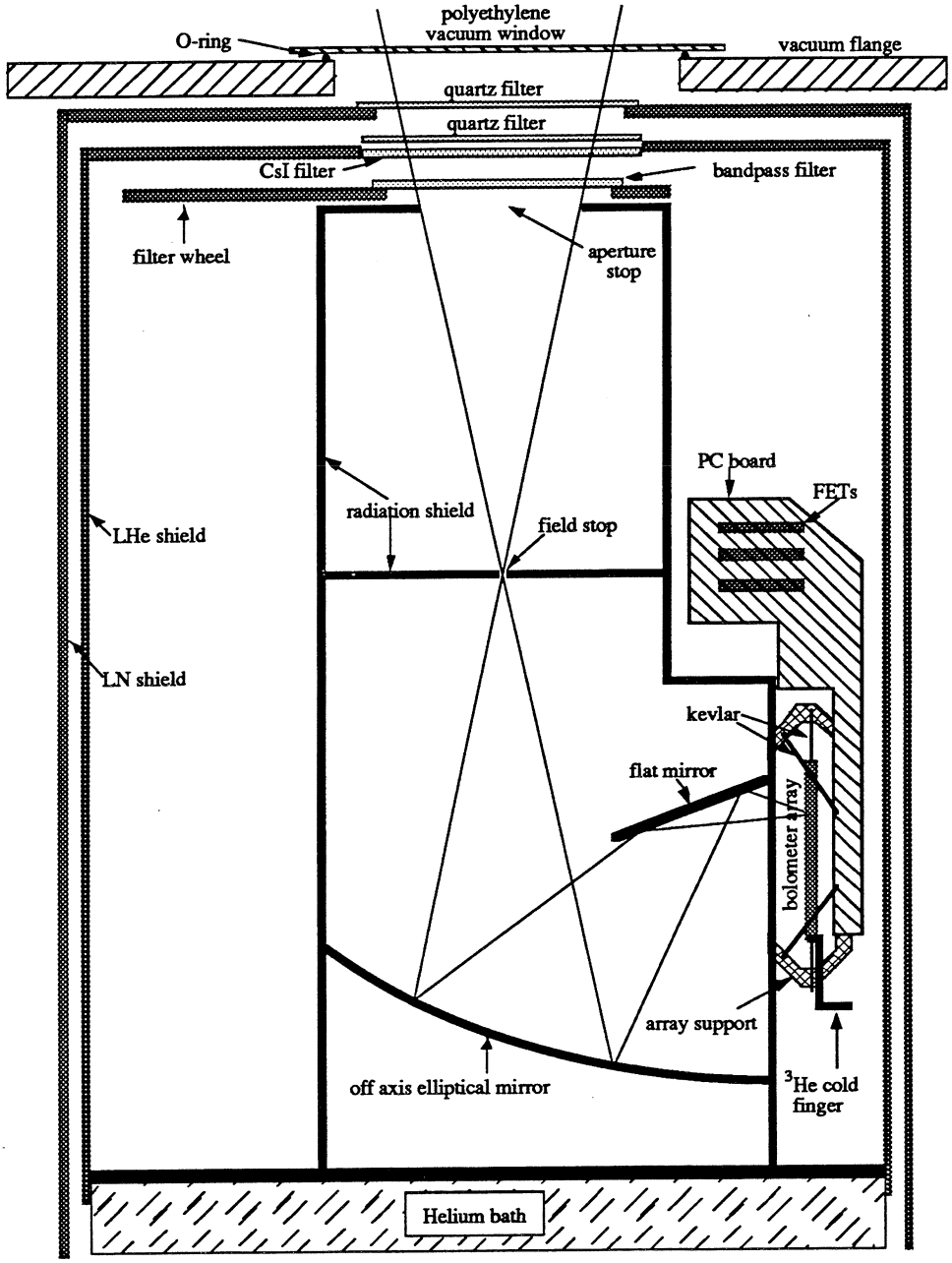

Figure 6. Schematic diagram of the CSO submillimeter high angular resolution camera, 'SHARC'.

The camera is used to observe in the 350 μm and 450 μm atmospheric windows at the CSO. We have purchased 350 μm and 450 μm resonant metal mesh bandpass filters from Cochise Instruments, Inc.[10], with a clear

aperture of 46 mm; these filters are made of layers of mylar with a copper mesh pattern deposited on one side of each layer. They are designed with a bandpass width matching the width of the atmospheric windows available from Mauna Kea (altitude 14,000'), the site of the CSO. One selects a filter by turning a shaft from outside the cryostat. We can install four such filters on the filter wheel. Currently a 350 μm and a 450 μm bandpass filter are mounted on the wheel, and the other two positions are used for diagnosing the system.

In addition to the aperture stop and the field stop, we installed radiation baffles to further eliminate light leaks. This is achieved by enclosing the cold imaging optics in a box, as shown in Figure 10. In order to reduce the scattered and reflected radiation from the surfaces of the baffling, the slit, the aperture stop, and the helium radiation shield, we painted them with Z306 Aeroglaze (Lord Corporation Industrial Coatings[11]). We add to the paint, by volume, 3% carbon black and 11% solid glass beads, with a mean diameter of 200 μm (Potters Industries, Inc.[12]). We have tested the reflectivity of this paint on aluminum and copper surfaces using the SIS receivers at the CSO, and found it to be about 35%. With such a configuration of light baffles, the only radiation coming from the vacuum window that can reach the bolometer array is that which passes through the aperture stop and the slit.

It is important to eliminate any radiation from 300 K parts or 130 K FETs. Because the photon energy is high from these sources, even when the photon flux is small, exerting little excess power load on the bolometer, the fluctuation of such a flux can be very large, dominating the NEP of the system. Therefore, in addition to having an enclosed box, we found that it is necessary to baffle around the ^{3}He pot, where there could be direct light passage from the heat switches to the bolometer array, in order to prevent 300 K radiation from the heat switches from reaching the bolometer. Furthermore, we installed baffles around the filter wheel shaft, and put the FETs in light tight housings which are heat sunk to the ^{4}He bath.

6. Characteristics of the Camera

When constructing an instrument for a ground based telescope, the aim is to have the instrument's sensitivity limited by the fluctuation of the background radiation from the sky. For a bolometer instrument, this means that the bolometer's responsivity needs to be high and that the system's electrical noise needs to be low.

Assume that the noise equivalent power from the fluctuation of the background radiation is NEP_{bkgd} $(W/\sqrt{Hz})$, the optical responsivity of the instrument is $\Re$ (V/W), and the voltage noise of the entire system is e_n $(V/\sqrt{Hz})$. The noise equivalent power of the instrument is thus

$$NEP = \frac{e_n}{\Re}. \qquad (4)$$

In order for the instrument to be background limited, the instrument's optical responsivity needs to satisfy $NEP << NEP_{bkgd}$.

A. Background Noise

The background noise comes from the fluctuations of the sky's blackbody radiation at around 280 K. The noise equivalent power can be estimated by [13, 14]

$$NEP_{bkgd} = \sqrt{\frac{4\varepsilon h\nu k_B T_B \Delta\nu}{\eta}\left(1+\varepsilon\eta\frac{k_B T_B}{h\nu}\right)} \qquad (5)$$

where ε is the emissivity of the sky, h is Planck's constant, υ is the radiation frequency, k_B is Boltzmann's constant, T_B is the temperature of the background radiation, $\Delta\upsilon$ is the bandwidth of the bandpass filter, and η is the total quantum efficiency of the system. For reasonable weather, with $\varepsilon = 0.5$, $T_B = 280$ K, a quantum efficiency of 10%, we find $NEP_{bkgd} \approx 2\cdot10^{-15}\ W/\sqrt{Hz}$ at 450 μm for a bandwidth of 100 GHz. In actuality, the edges of the atmospheric window are poorer, so a more accurately calculated value is $NEP_{bkgd} \approx 4\cdot10^{-15}\ W/\sqrt{Hz}$.

B. Optical Responsivity

We have measured the optical responsivity of the camera in the laboratory. A room temperature elliptical mirror was mounted on the bottom of the cryostat to reimage the slit inside the cryostat onto an external chopper wheel. The chopper wheel chopped at 10 Hz between 300 K and 77 K sources. For our 450 μm bandpass filter, we expect a chopped signal of 240 pW on each bolometer, estimated using the expression of $2k_B T\left(A\Omega/\lambda^2\right)\Delta\nu$, where A is the area of the bolometer pixel, Ω is the solid angle that the pixel subtends to the aperture stop, λ is the wavelength, and Δυ is the bandwidth of the bandpass filter, which is about 100 GHz for both the 350 μm and the 450 μm filters. At 450 μm, the signal observed on all the pixels is about 2.2 mV peak-to-peak, resulting in an optical responsivity of $9\cdot10^6\ V/W$. Similarly, for the 350 μm filter, the input power at the vacuum window is about 400 pW, and the peak to peak signal is about 4.6 mV, giving an optical responsivity of $1\cdot10^7\ V/W$.

C. Total Quantum Efficiency of the Camera

We have measured the total quantum efficiency of the camera. We record the pixels' I-V curves when we expose the polyethylene window to 300 K and 77 K radiation, respectively. From the zero bias resistance, one can obtain the temperature of the bolometer pixel. Using the thermal conductance G(T) measured earlier, one can estimate the power absorbed by the pixel,

$$P = \int_{T_{sink}}^{T_{bolo}} G(T)dT\,. \qquad (6)$$

The power absorbed by each pixel with the 450 μm filter in place is 34 pW when the bolometers are exposed to 300 K radiation, and 13 pW when they are exposed to 77 K radiation. Compensating for excess power on the pixel from surrounding walls and some possible small light leaks, the quantum efficiency is estimated using the ratio of the power difference between 300 K and 77 K radiation. This gives a total quantum efficiency in the 450 μm window of about 9%, and 10% in the 350 μm window.

From the measured impedance of the bismuth film at 4 K, we anticipate a 30% absorptivity for the bolometers alone. The polyethylene window is expected to transmit about 90%, as is the 450 μm bandpass filter. The infrared blocking filters are expected to have a transmission rate of about ~50% together. The product of all of these transmissions gives an estimated total quantum efficiency of about 12%. If we assume that the emissivity of the sources is about 90%, the expected quantum efficiency is about 11%. The measured value of 9-10% is therefore reasonable.

D. NEP of the Camera

We have measured the noise of one pixel, using a spectrum analyzer, when tau is 0.03 at 225 GHz and the telescope is staring at a blank piece of sky at a zenith angle of about 45 degrees. The noise at 4 Hz is about 50 $nV/\sqrt{Hz}$, which gives

$$NEP = \frac{e_n}{\Re} \approx \frac{50 \cdot 10^{-9}}{1 \cdot 10^{7}} \frac{(V/\sqrt{Hz})}{(V/W)} = 5 \cdot 10^{-15} \quad W/\sqrt{Hz} \tag{7}$$

This is close to the expected background noise, so the camera is approximately background limited.

With the measured optical responsivity of $1 \cdot 10^{7}$ V/W and a background NEP of $4 \cdot 10^{-15}$ $W/\sqrt{Hz}$, one needs to achieve a voltage noise less than 40 $nV/\sqrt{Hz}$ in order to be background limited. We can see from Figure 10 that the voltage noise of the bolometer is about 20 $nV/\sqrt{Hz}$ when the bias is grounded. As soon as we apply a bias voltage on, the noise increases to about 50 $nV/\sqrt{Hz}$. Because this excess noise is present only when the bias is on, it is probably caused by a light leak. Given that the careful baffling against 300 K radiation was done, we suspect that the possible source of this light leak is the heated FETs. We are in the process of eliminating this excess noise to make the camera background limited.

E. NEFD of the Camera

We have made an independent measurement of the noise equivalent flux density (NEFD) above the atmosphere, at 350 μm, from observations of Uranus at an airmass of 1.33. The average optical depth across the camera filter bandpass measured directly from the dependence of the observed intensity of Saturn as a function of the airmass was 0.6. At the time when this data was taken, about 50% of the noise in the map is correlated among all the pixels. This correlated component can be removed, though not completely, in data reduction software. The remaining uncorrelated noise component gives an NEFD of about 4-9 $Jy/\sqrt{Hz}$ over different parts of the map. Since then, we have eliminated the source of the correlated noise, and the RMS noise has improved by at least a factor of 2. Unfortunately, Uranus is unavailable for recalibration. Based in the signal-to-noise ratio on known sources, we estimate the camera's NEFD to be around 4 $Jy/\sqrt{Hz}$ under good weather conditions. Given the measured NEP, we can then calculate the expected NEFD at the CSO; an NEP of $5 \cdot 10^{-15}$ $W/\sqrt{Hz}$ is equivalent to an NEFD of 3.5 $Jy/\sqrt{Hz}$, a very consistent result.

F. Calibration of the Bolometer Pixels

We have checked the relative sensitivity of all the pixels by pointing each pixel towards Saturn and recording the signal; the Signal to noise ratio varies by about a factor of 2 from pixel to pixel. For observing astronomical sources, it is also important to know the relative gain of all the pixels, which is well characterized by the peak value from each pixel when Saturn is maximally illuminating that pixel. The variation on the gain among all the pixels is about 30%, much smaller than that of the SNR.

G. Light Leaks

In a design that does not use Winston cones, it is crucial to eliminate all the light leaks with baffles. Despite baffling around all optical components, there is still a light leak through the vacuum window which is around 0.1% of the 350 μm signal size when chopping between 300 K and 77 K. Also, there may be a light leak from the separately baffled warm FETs, which could explain the excess noise seen with the bias on.

H. Optical Performance

We have checked pointing and focus on Saturn, which all came out to be very reasonable. In order to check the alignment between the optical components, we scanned Saturn in both azimuth and zenith angle. The full width at half maximum in both directions coincides well with the size of Saturn, convolved with the telescope Airy pattern and taking into the finite size of the pixel, indicating that the camera is diffraction limited, as expected. Since each pixel subtends 5 arcseconds by 10 arcseconds on the sky, and the diffraction limited beam size is about 10 arcseconds at 400 μm, we therefore have Nyquist sampling along the length of the array at 350 and 450 μm, as the gap between two adjacent pixels is only 0.075 arcseconds on the sky.

We have made an On-The-Fly map of NGC 2024 at 350 μm, shown in Figure 7. The data were taken in October 1995 by scanning at constant elevation so that all the pixels crossed the source. The atmospheric opacity was tau = 0.05 at 225 GHz, observed at an airmass of 1.1 - 1.2, with a chopping frequency of 4 Hz and a chop throw of 48 arcseconds. The dual beam scans were restored using the NOD-2 algorithm and then interpolated onto a regular grid in equatorial coordinates. The resultant map is the sigma weighted average of the data from all the pixels, with an RMS noise level of about 3.5 Jy and an effective angular resolution of approximately 11 arcseconds.

7. Conclusion

We have constructed a submillimeter continuum camera operating in the 350 and 450 μm atmospheric windows. It has an optical responsivity of $1 \cdot 10^{7}\ V/W$, a total quantum efficiency of 10%, and an optical NEP of about $5 \cdot 10^{-15}\ W/\sqrt{Hz}$. In good weather (tau at 225 GHz of 0.03 at 1.33 airmasses) the camera NEFD is about 4 $Jy/\sqrt{Hz}$. The linear array of 24 bolometer pixels Nyquist sample the diffraction beam, imaging a strip of sky 10 arcseconds wide and 2 arcminutes long. However, the camera has not yet reached its optimal sensitivity, as there still exist some excess noise related to bias. We are in the process of trying to eliminate this noise to make the camera background limited.

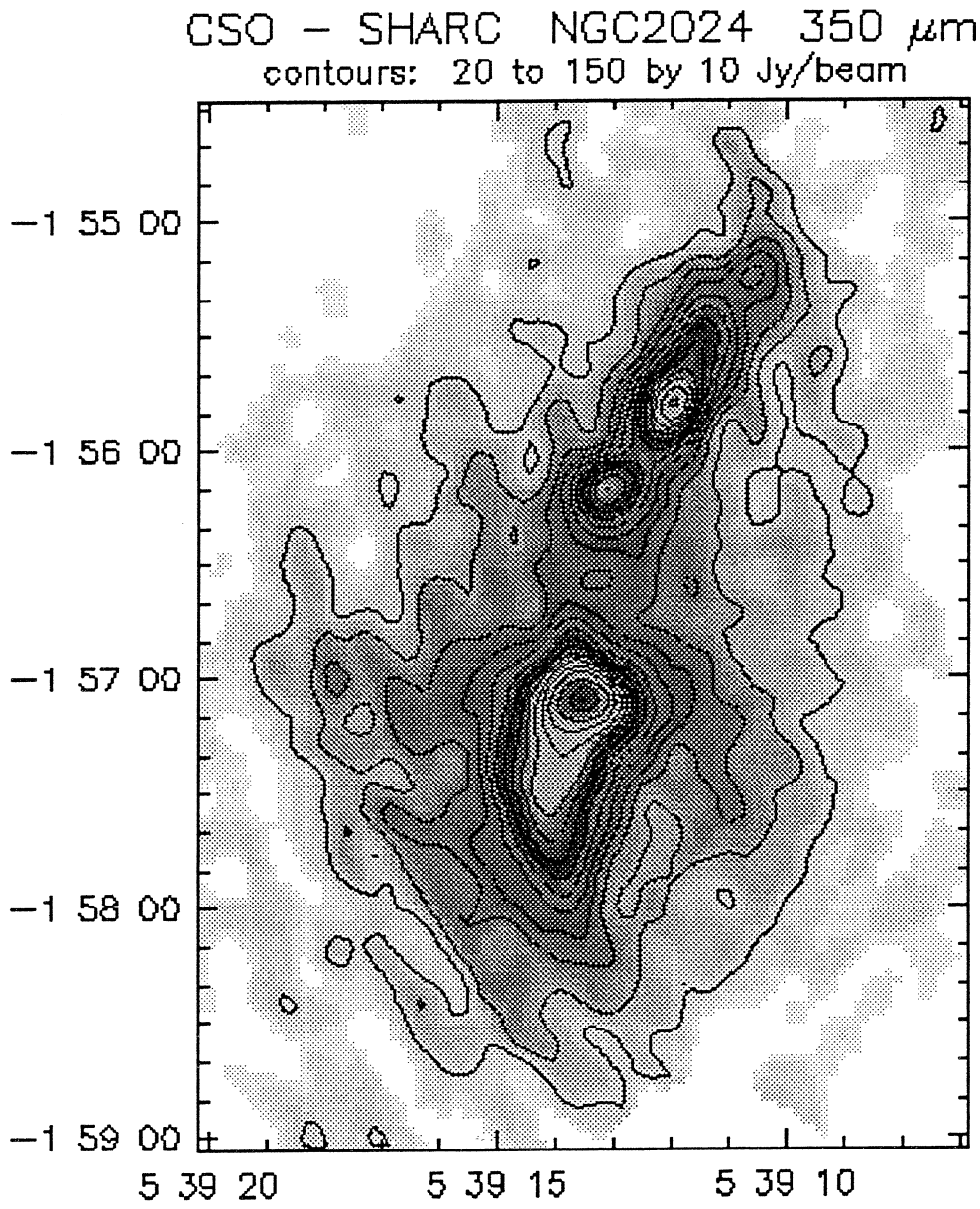

Figure 7. Greyscale image of the 350 μm emission toward NGC 2024, a star forming region located in the Orion Molecular Cloud.

Acknowledgments

We want to thank the people in the microelectronics lab at the GSFC, R. Kelly and S. Murphy for FET work, J.B. Keene for discussions on filters, B. Smith for wiring the circuit boards, and A. Cleland for helping out with many tests in the laboratory and for many discussions on bolometer physics. We are grateful for all the help from the CSO staff, in particular, A. Schinckel, K. Young, A. Guyer, and M. Houde. This work is supported by NSF grant AST-9313929. D.J. Benford is supported by a NASA Graduate Student Research Fellowship.

Refeferences

1 N. Wang, T.R. Hunter, D.J. Benford, E. Serabyn, D.C. Lis, T.G. Phillips, S.H. Moseley, K. Boyce, A. Szymkowiak, C. Allen, B. Mott, and J. Gygax, *Appl. Opt.* 1996, submitted.

2 D. A. Harper, R. H. Hilderbrand, R. Stiening, and R. Winston, *Appl. Opt.* **15**, 53 (1976).

3 S.H. Moseley, J.C. Mather, D.J. McCammon, *J. Appl. Phys.* **56**(5) 1257 (1984).

4 J. Clarke, G.I. Hoffer, P.L. Richards, and N. -H. Yeh, *J. Appl. Phys.* **48**(12) 4865 (1978).

5 R.C. Jones, *J. Opt. Soc. Am.*, **43**, 1-14 (1953).

6 J.G. Hust, *Cryogenics*, March, 126-128(1975).

7 A. L. Efros and B. I. Shklovskii, *Electronic Properties of the Doped Semiconductors* (Springer-Verlag, New York, 1984).

8 InterFET, 322 Gold Street, Garland, TX 75042;(214) 487-1287.

9 Infrared Laboratories, 1808 East 17th Street, Tucson, AZ 85719; (602) 622-7074.

10 Cochise Instruments, Inc., 6304 deMello Street, Hereford, AZ 85615; (602) 378-6321.

11 Lord Corporation Industrial Coatings, 2000 West Grandview Blvd., P.O. Box 10038, Erie, PA 16514-0038; (814) 868-3611.

12 Potters Industries, Inc., Waterview Corporate Centre, 20 Waterview Blvd., Parsippany, NJ 07054-1282; (201) 299-2900, Part #: A-glass 1922 and 2024.

13 T. G. Phillips, in Millimeter and Submillimeter Astronomy, p1-25, edited by R. D. Wolstencroft and W. B. Burton (Kluwer Academic Publishers, 1988).

14 N. Wang, T.R. Hunter, D.J. Benford, E. Serabyn, T.G. Phillips, and S.H. Moseley, Proceedings of SPIE, *Instrumentation in Astronomy VIII*, 13-14 March 1994, Kona, Hawaii, **2198**, p749-756.